INSTITUTE OF PHYSICS PUBLISHING JOURNAL OF PHYSICS: CONDENSED MATTER

J. Phys.: Condens. Matter **16** (2004) S1957–S1968 PII: S0953-8984(04)73367-6

Dynamics of a nematic liquid crystal around a spherical particle

Jun-ichi Fukuda[1], **Holger Stark**[2], **Makoto Yoneya**[1] **and Hiroshi Yokoyama**[1,3]

[1] Yokoyama Nano-structured Liquid Crystal Project, ERATO, Japan Science and Technology Agency, 5-9-9 Tokodai, Tsukuba 300-2635, Japan
[2] Fachbereich Physik, Universität Konstanz, D-78457 Konstanz, Germany
[3] Nanotechnology Research Institute, AIST, 1-1-4 Umezono, Tsukuba 305-8568, Japan

E-mail: fukuda@nanolc.jst.go.jp

Received 11 December 2003
Published 30 April 2004
Online at stacks.iop.org/JPhysCM/16/S1957
DOI: 10.1088/0953-8984/16/19/008

Abstract

We present the results of our numerical calculations that focus on the dynamics of a nematic liquid crystal around a spherical particle imposing strong homeotropic anchoring at the surface. The first part of this article is devoted to the discussion of the effect of an external magnetic or electric field on the director configuration of a nematic liquid crystal. With the aid of an adaptive mesh refinement scheme, together with the tensor description of the orientational order, for the first time in numerical calculations we successfully reproduce the transition from a hyperbolic hedgehog defect to a Saturn ring defect, which was observed in a recent experiment. We also find that the trajectories of the defect core sensitively depend on the field strength. In the second part we investigate how a hydrodynamic flow influences the orientational order of a nematic liquid crystal around a particle carrying a hyperbolic hedgehog defect. We observe that for an intermediate Ericksen number, which characterizes the ratio of the viscous force to the elastic force of a nematic liquid crystal, the liquid crystal is strongly convected by the flow, which results in a considerable elastic distortion.

1. Introduction

Liquid crystal colloid dispersions provide a novel class of composite materials and have attracted considerable interest in the technology as well as in the fundamental science [1–6]. Most of the fascinating properties of liquid crystal colloid dispersions arise from the elastic distortion of a liquid crystal due to the surface anchoring of the dispersed particles or droplets [7–10]. Various kinds of superstructures formed by particles such as linear chains [2] and periodic lattices [6] are attributed to the interaction between particles mediated by the elastic deformation of a liquid crystal surrounding them.

Another interesting property of liquid crystal colloid dispersions is that topological defects accompany particles to preserve the neutrality of topological charges when the anchoring of the surface of the particles and the resultant deformation of a liquid crystal are strong enough [2, 11, 12]. Experimentally observed defects include a point-like defect called a hyperbolic hedgehog [11], a Saturn ring that surrounds a particle as the name implies [12, 13], and two surface defects located at the poles of the particles known as boojums [11]. The understanding of the condition for the creation of these various defects has been an important problem of liquid crystal science, because topological defects have long been one of the fundamental subjects of condensed matter physics, and liquid crystals have been extensively studied as one of the experimentally accessible systems showing a rich variety of topological defects. It is also because the interaction between particles and the resultant superstructures sensitively depend on what kind of topological defects accompany the particles.

There have been several numerical attempts [14–20] to investigate the properties of topological defects in a nematic liquid crystal around a particle. Several authors [21, 22] have also been developing numerical schemes that can simulate liquid crystals containing two or more mobile particles. However, the system possesses two characteristic lengths; one is the size of the particles of the order of micrometres and the other is the coherence length of the liquid crystal, which is of the order of the size of the topological defect cores ($\sim$10 nm). The coexistence of these largely different length scales makes the numerical problem highly challenging. Most of the previous studies deal with the orientational order using a director description $\boldsymbol{n}$, where the core of a topological defect has to be treated as a singular point and the introduction of some cutoff is inevitable. Moreover, since the numerical resolutions in the previous studies are insufficient, 'numerical pinning' of the topological defects occurs, which makes it almost impossible to investigate the dynamical behaviour of topological defects.

In our previous studies [18–20], we have employed the description of the orientational order in terms of a second-rank tensor $Q_{\alpha\beta}$, which allows a direct treatment of topological defects without introducing any singularities. Moreover, to overcome the numerical difficulties arising from the large difference between the size of a particle and that of the core of a topological defect, we have devised an adaptive mesh refinement scheme, where fine numerical grids are assigned only around topological defects and sufficient numerical resolution is achieved with greatly reduced resources. We have already shown that the numerical resolution is fine enough to observe the detailed structure of a ring-like hyperbolic hedgehog [19]. We have also presented the dynamical simulation of the splitting of a -1 topological defect into two defects with charge $-1/2$ around a circular particle in two dimensions [18]. We emphasize that this was the first numerical study exhibiting successfully the dynamical behaviour of a topological defect around a particle.

This paper focuses on the dynamics of the liquid crystal orientation profile together with the topological defects around a spherical particle when an external perturbation is applied to the system. In the first part of this paper, section 2, we present our numerical results under the application of an external magnetic or electric field. It was predicted by Stark [15] that a hedgehog configuration becomes energetically unstable compared with a Saturn ring under the application of an external magnetic or electric field parallel to the symmetry axis. Loudet and Poulin [23] later confirmed this prediction experimentally by observing the transition from a hedgehog to a Saturn ring under an electric field. They also found that after the cessation of the field a Saturn ring becomes unstable and shrinks to a hedgehog when the particle radius is sufficiently large [24]. However, the argument in [15] was based on the comparison of the free energy for the two configurations, and the dynamics of topological defects in the transition process was never discussed. In our previous study [20], we successfully reproduced the dynamics of the transition from the hedgehog to the Saturn ring configuration in computer

simulations for the first time. In this paper we will give a more detailed argument on the motion of the topological defect in the transition process.

The second part, section 3, is devoted to the discussion of the effect of a uniform hydrodynamic flow on the liquid crystal orientation. Because of the coupling between the orientational order and the fluid velocity, the hydrodynamics of a liquid crystal is far more complicated than that of a usual isotropic fluid and, even in a simple geometry such as a uniform shear, the response of a liquid crystal is not at all trivial, depending on the relative orientation of the flow direction, the shear direction and the director [25]. The hydrodynamic behaviour of liquid crystal colloidal dispersions is even more complex and provides a challenge to theoretical and computational physicists. There have been several numerical attempts [26–30] to deal with the hydrodynamics of a nematic liquid crystal around a particle. However, many of them assumed that the equilibrium director profile is not distorted by the flow because the fluid velocity is small enough or a strong external field is applied. Only very few studies [28, 30] discussed how the director profile around a particle or a cylinder is influenced by the imposed flow. Moreover, those previous studies calculated only the stationary profiles of the director and the fluid flow. So far as we know, none of them dealt with the dynamical behaviour, or the relaxation process to a stationary state of the director and the fluid flow, which is the main subject of section 3. We will give a brief conclusion in section 4.

2. Field-induced transition of a topological defect

In this section, we present our numerical results as to how an external magnetic or electric field affects the orientation profile of a nematic liquid crystal around a spherical particle. To describe the orientational order, we use, as in our previous studies [18–20], a second rank tensor $Q_{\alpha\beta}$ that satisfies $\mathrm{Tr}\,\mathsf{Q} = Q_{\alpha\alpha} = 0$ (hereafter summations over repeated indices are implied). The employment of the tensor order parameter is consistent with the head–tail ($\boldsymbol{n} \leftrightarrow -\boldsymbol{n}$) symmetry of a nematic. Moreover, with the tensor description we do not have to treat the cores of topological defects as singularities as in the director description.

The free energy density in terms of the order parameter $Q_{\alpha\beta}$ is written as $f = f_{\mathrm{bulk}}(Q_{\alpha\beta}) + f_{\mathrm{el}}(Q_{\alpha\beta}, \nabla) + f_{\mathrm{ext}}(Q_{\alpha\beta}, \tilde{H}_\alpha)$, where $f_{\mathrm{bulk}}(Q_{\alpha\beta})$ is the bulk local energy, $f_{\mathrm{el}}(Q_{\alpha\beta}, \nabla)$ is the elastic energy due to the distortion of the orientation profile, and $f_{\mathrm{ext}}(Q_{\alpha\beta}, \tilde{H}_\alpha)$ is the energy due to an external (magnetic or electric) field $\tilde{\boldsymbol{H}}$. In terms of the Landau–de Gennes expansion, the bulk energy f_{bulk} reads

$$f_{\mathrm{bulk}} = -\tfrac{1}{2}A\,\mathrm{Tr}\,\mathsf{Q}^2 + \tfrac{1}{3}B\,\mathrm{Tr}\,\mathsf{Q}^3 + \tfrac{1}{4}C(\mathrm{Tr}\,\mathsf{Q}^2)^2 + \lambda\,\mathrm{Tr}\,\mathsf{Q}, \tag{1}$$

where the last term ensures $\mathrm{Tr}\,\mathsf{Q} = 0$. As in the previous studies [19, 20] we set the phenomenological coefficients as $C = -B = 3A$ in this section, so that an order parameter with uniaxial symmetry

$$Q_{\alpha\beta} = Q_0\big(n_\alpha n_\beta - \tfrac{1}{3}\delta_{\alpha\beta}\big) \tag{2}$$

with $Q_0 = 1$ minimizes f_{bulk}. In equation (2), Q_0 serves as a scalar order parameter that describes the strength of the nematic order and a unit vector $\boldsymbol{n}$ corresponds to the director. In a simplified one-constant form, the elastic energy f_{el} is given by

$$f_{\mathrm{el}} = \tfrac{1}{2}L_1\partial_\gamma Q_{\alpha\beta}\partial_\gamma Q_{\alpha\beta} \tag{3}$$

with L_1 being the elastic constant. We adopt the following form for the energy f_{ext} due to the external field:

$$f_{\mathrm{ext}} = -\tilde{H}_\alpha\tilde{H}_\beta\frac{Q_{\alpha\beta}}{\sqrt{\mathrm{Tr}\,\mathsf{Q}^2}}. \tag{4}$$

Here we consider the situation that the director tends to be parallel to the field as the minus sign indicates. Notice that we have not used a usual form of the free energy $-\tilde{H}_\alpha \tilde{H}_\beta Q_{\alpha\beta}$ due to the external field. When we use $-\tilde{H}_\alpha \tilde{H}_\beta Q_{\alpha\beta}$, the scalar order parameter Q_0 in equation (2) that minimizes the bulk energy $f_{\rm bulk} + f_{\rm ext}$ will change according to the variation of the strength of the external field. This may cause a mismatch between the order parameter in the bulk and that at the particle surface, which is fixed as prescribed below. To avoid such a mismatch, we employ instead equation (4) as the free energy due to the external field (we note that substituting equation (2) into (4) yields $-(\sqrt{6}/2)(\tilde{\boldsymbol{H}} \cdot \boldsymbol{n})^2$ which is independent of Q_0. The scalar order parameter Q_0 that minimizes $f_{\rm bulk} + f_{\rm ext}$ is therefore independent of $\tilde{H}$). We are interested in the deep nematic state and not in the variation of the strength of the orientational order Q_0 due to the external field. We also notice that in the bulk $Q_{\alpha\beta}$ takes the form of equation (2) with fixed Q_0 throughout the system except the very small region around the defect core. Therefore the factor $1/\sqrt{\mathrm{Tr}\,\mathsf{Q}^2}$ in equation (4) just renormalizes the field strength.

The dimensionless field $\tilde{H}$ is associated with a dimensional one H as $\tilde{H}^2 = \Delta\chi H^2/\sqrt{6}$, with $\Delta\chi$ being the anisotropy of the susceptibility that is assumed to be positive. We note that a uniform field employed in the following numerical calculations can be more safely assumed in the case of a magnetic field than an electric field.

We assume that the anchoring is homeotropic and rigid at the particle surface with radius R_0 so that the order parameter becomes $Q_{\alpha\beta} = Q_{\rm s}(\nu_\alpha \nu_\beta - (1/3)\delta_{\alpha\beta})$ with $Q_{\rm s} = Q_0 = 1$ and $\boldsymbol{\nu}$ being a unit vector normal to the particle surface. Therefore, a surface energy does not appear in our system. As the boundary condition at infinity, we set $Q_{\alpha\beta} = Q_0(e^z_\alpha e^z_\beta - (1/3)\delta_{\alpha\beta}) = Q_0(\delta_{z\alpha}\delta_{z\beta} - (1/3)\delta_{\alpha\beta})$, where $\boldsymbol{e}^z$ is a unit vector parallel to the z-axis. Therefore, we consider a case where a particle is immersed in a nematic liquid crystal uniformly aligned along the z direction. We also assume rotational symmetry about the z-axis, which renders the numerical problem an effectively two-dimensional one.

In this section we use the following simplified relaxation equation for the dynamics of the orientational order, although we will deal with a full set of hydrodynamic equations in the next section:

$$\frac{\partial}{\partial t} Q_{\alpha\beta}(\boldsymbol{r}) = -\Gamma \frac{\delta F}{\delta Q_{\alpha\beta}(\boldsymbol{r})}, \tag{5}$$

where $F = \int \mathrm{d}\boldsymbol{r}\, f$ is the total free energy of the system and Γ, assumed to be a constant, is a kinetic coefficient associated with the rotational viscosity. Further details of the numerical calculations are given in our previous articles [19, 20].

Before presenting our numerical results, we notice that the system possesses two characteristic lengths apart from the particle radius R_0, and we will express them as dimensionless quantities in units of R_0. One is the nematic coherence length defined as $\xi = \sqrt{L_1/A}/R_0$ and the other is the magnetic coherence length $\xi_H = \sqrt{L_1/\tilde{H}^2}/R_0$. In the following numerical calculations, we have set $\xi = 3.65 \times 10^{-3}$ ($\xi^2 = 1.33 \times 10^{-5}$), for which the hedgehog configuration is stable when no external field is applied and the equilibrium profile of the hedgehog configuration is used as the initial condition. Note also that from the definition ξ_H^{-1} is proportional to $\tilde{H}$ and can be regarded as a reduced field strength.

In figure 1, we show the time evolution of the orientation profile from the equilibrium hedgehog configuration after the application of the external field parallel to the symmetry axis (z-axis) at $t = 0$. Grey-scale plots of Q^2_{zz} are employed and in the black regions, the director is parallel to the z-axis. Therefore the effect of the external field manifests itself in the larger black regions after its application (we note again that we consider the cases with positive $\Delta\chi$, where the director tends to align parallel to the field). When the field is weaker than some threshold value ($\xi_H^{-1} \simeq 10.6$), the hedgehog configuration is stable as can be seen

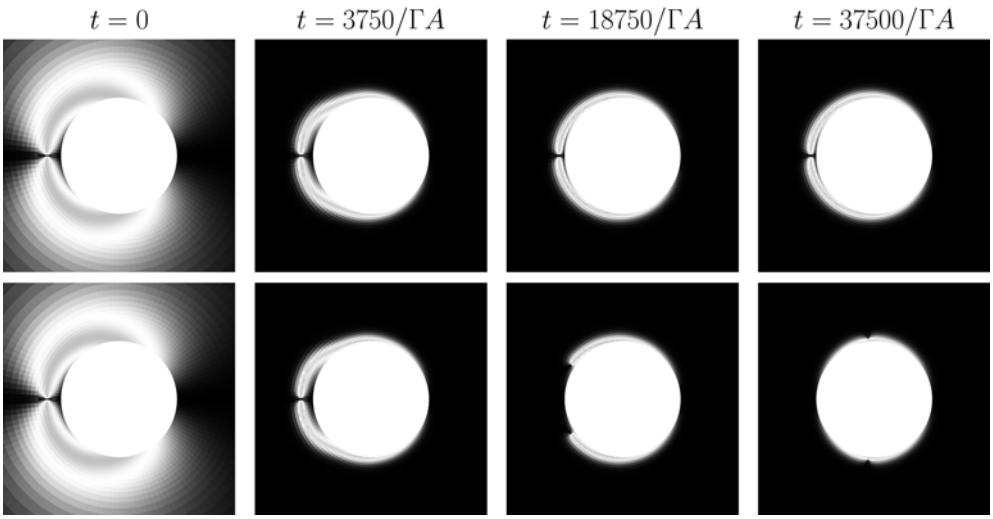

Figure 1. Time evolution of the orientation profile (grey-scale plots of Q^2_{zz}). The z-axis, which is parallel to the symmetry axis and the field direction, is along the horizontal direction. The numbers indicate the time after the application of the field. The first and the second rows show the results for $\xi_H^{-1} = 10.0$ and 11.0, respectively.

in the first row of figure 1 with $\xi_H^{-1} = 10.0$. We can also find that the hedgehog defect moves closer to the particle after the application of the field. When the field is strong enough, the hedgehog configuration becomes unstable. The hedgehog defect is originally made up of a small ring [19] and its radius grows with time. Eventually the orientation profile takes a Saturn ring configuration, although this may be hard to observe from figure 1 because the defect is too close to the particle. This result qualitatively reproduces the experiment by Loudet and Poulin [23] who observed the transition of a hedgehog to a Saturn ring by the application of an electric field.

To observe the motion of the defect more clearly, we show in figure 2 the trajectories of the defect cores for different field strengths larger than the threshold value for the transition. When the field is weak and close to the threshold value ($\xi_H^{-1} = 11.0$), the defect first moves closer to the particle without opening up, or in other words, while retaining the hedgehog configuration, and afterwards it opens up to transform to a Saturn ring. However, under a stronger field ($\xi_H^{-1} = 12.6$), the approaching of the defect to the particle and the opening up of the defect occur simultaneously. When we increase the field strength further ($\xi_H^{-1} = 14.1$), the defect opens up first without approaching the particle, and afterwards the distance of the defect to the particle surface decreases gradually. The difference in the transition process for different field strength is significant and we believe that the experimental resolution is fine enough to detect it.

We also find from figure 2 that the motion of the defect becomes slower when the Saturn ring configuration is approached. It is obvious from the consideration of the symmetry that the force acting on the topological defect from the elastic deformation of the liquid crystal is zero just at the Saturn ring configuration. Indeed, Loudet *et al* [24] reported that the motion of the defect is very slow when the deviation from the Saturn ring configuration is small enough, although their experimental situation is different from ours; they observed the transition process from the Saturn ring to the hedgehog configuration after the cessation of the external field.

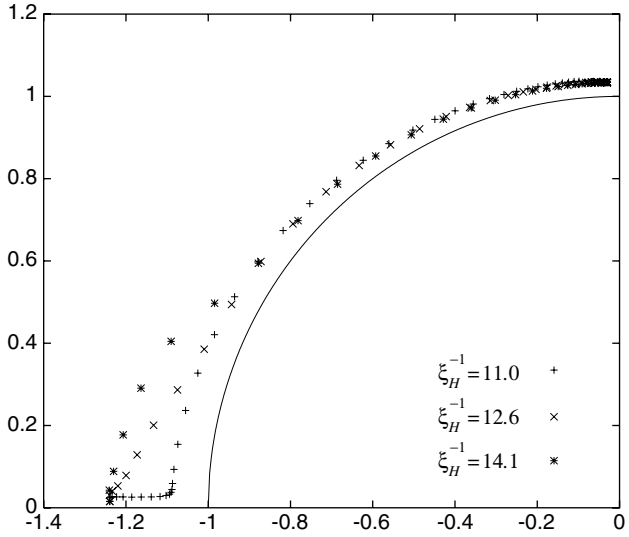

Figure 2. Trajectories of the topological defect after the application of the field for different field strengths. The z-axis is along the horizontal direction and the arc is a part of the particle surface. The unit of the length is the particle radius R_0. The time interval between two adjacent points is $937.5/\Gamma A$ for all ξ_H^{-1}.

3. Effect of hydrodynamic flow on the liquid crystal configuration

In this section, we present some preliminary results on the effect of a uniform hydrodynamic flow on the director configuration of a nematic liquid crystal around a spherical particle. Here we give only the outline of the model employed; the details of the numerical calculations will be presented elsewhere.

A spherical particle with radius R_0 is fixed so that the centre of the particle is located at the origin of the coordinate system. As in the previous section, strong homeotropic anchoring is imposed at the surface of the particle and the order parameter $Q_{\alpha\beta}$ is uniaxial and fixed, with the principal eigenvector of $Q_{\alpha\beta}$ being parallel to the surface normal (or the radial unit vector $\boldsymbol{e}_{\mathrm{r}}$). The degree of orientational order at the surface is the same as that in the bulk. The orientational order at infinity is taken to be uniform and parallel to the z-axis. We impose a uniform flow with speed v_∞ at infinity that is parallel to the z-axis (or the orientational order). A no-slip boundary condition at the particle surface is employed, so that $\boldsymbol{v} = \boldsymbol{0}$ there. As in the previous section, we also assume here that the system possesses rotational symmetry about the z-axis and therefore the numerical problem is an effectively two-dimensional one.

There have been several theoretical attempts to formulate the hydrodynamic equations for the velocity $\boldsymbol{v}(\boldsymbol{r})$ and the tensor order parameter field $Q_{\alpha\beta}(\boldsymbol{r})$ of a nematic liquid crystal [31–35]. We use those given by Olmsted and Goldbart [32], which are written, after some appropriate rescaling of the length, the time, and the order parameter $Q_{\alpha\beta}$, as

$$Re\left(\frac{\partial}{\partial t} + \boldsymbol{v}\cdot\boldsymbol{\nabla}\right)v_\alpha = \partial_\gamma\left[2\kappa^{[\mathrm{s}]}_{\alpha\gamma} + \frac{1}{Er^*}(-\overline{\beta}_1 H^{[\mathrm{s}]}_{\alpha\gamma} + \sigma^{i[\mathrm{a}]}_{\alpha\gamma} + \sigma^{d}_{\alpha\gamma}) - p\delta_{\alpha\gamma}\right], \tag{6}$$

$$\left(\frac{\partial}{\partial t} + \boldsymbol{v}\cdot\boldsymbol{\nabla}\right)Q_{\alpha\beta} - (\kappa^{[\mathrm{a}]}_{\alpha\gamma}Q_{\gamma\beta} - Q_{\alpha\gamma}\kappa^{[\mathrm{a}]}_{\gamma\beta}) = \overline{\beta}_1\kappa^{[\mathrm{s}]}_{\alpha\beta} + \frac{1}{\overline{\beta}_2 Er^*}H^{[\mathrm{s}]}_{\alpha\beta}. \tag{7}$$

Here the units of length and time are R_0 and R_0/v_∞, respectively. The velocity gradient tensor is $\kappa_{\alpha\beta} \equiv \partial_\alpha v_\beta$. The superscripts [s] and [a] denote the symmetric and the anti-symmetric

components of a second-rank tensor, respectively. $H_{\alpha\beta} \equiv -\delta F/\delta Q_{\alpha\beta}$ is the molecular field with F being the free energy of the system. The precise form of $H_{\alpha\beta}$ after rescaling will be given below. $\sigma^{i[a]}_{\alpha\beta} = H^{[s]}_{\alpha\gamma} Q_{\gamma\beta} - Q_{\alpha\gamma} H^{[s]}_{\gamma\beta}$ is the anti-symmetric component of the stress tensor arising from the coupling between the orientational order and the flow. The elastic stress is given by $\sigma^{d}_{\alpha\beta} = -(\partial F/\partial(\partial_\alpha Q_{\mu\nu})) \times \partial_\beta Q_{\mu\nu}$. The rescaled kinetic coefficient $\overline{\beta}_1$ is associated with the off-diagonal kinetic coupling between $Q_{\alpha\beta}$ and $\boldsymbol{v}$. Another kinetic coefficient $\overline{\beta}_2$ is the rescaled rotational viscosity.

After the rescaling, the molecular field $H_{\alpha\beta}$ reads

$$H_{\alpha\beta} = -\tau Q_{\alpha\beta} + \frac{3\sqrt{6}}{4} Q_{\alpha\gamma} Q_{\gamma\beta} - (\mathrm{Tr}\, \mathsf{Q}^2) Q_{\alpha\beta} + {\xi_R}^2 \nabla^2 Q_{\alpha\beta} + \lambda \delta_{\alpha\beta}, \tag{8}$$

where the external field $\tilde{H}$ is set to zero and we employ a definition of the (dimensionless) nematic coherence length different from that in the previous section: $\xi_R \equiv \sqrt{L_1/Cs^2}/R_0$ with $s \equiv 2\sqrt{6}|B|/9C$ being a variable appearing in the rescaling of the order parameter. As the reduced temperature, we choose $\tau = (3\sqrt{6} - 8)/12$, so that an order parameter with uniaxial symmetry, equation (2) with $Q_0 = 1$, minimizes the bulk energy.

One of the important dimensionless quantities characterizing the problem is the ratio of viscous force to the elastic force of a nematic liquid crystal:

$$Er = \frac{Er^*}{{\xi_R}^2} = \frac{\beta_3 v_\infty R_0}{2s^2 L_1}, \tag{9}$$

where β_3 is associated with the isotropic part of the viscosity whose precise definition can be found in [32]. Er is nothing more than the Ericksen number apart from the numerical factor. The Reynolds number $Re = 2\rho v_\infty R_0/\beta_3$, with ρ being the mass density of the liquid crystal, is much smaller than unity in our problem dealing with a micrometre-size particle and set to zero in our calculations.

Using the material parameters in [32], we set $\overline{\beta}_1 = 1.4$ and $\overline{\beta}_2 = 2$. The dimensionless nematic coherence length is $\xi_R = 5 \times 10^{-3}$, which corresponds to taking $R_0 \simeq 3$ μm when we use the material parameters of [32] again. For $R_0 = 3$ μm, the Ericksen number is $Er \simeq 1.2 \times 10^{-2} \times (v_\infty\ (\mu\mathrm{m\ s^{-1}}))$. Therefore, to achieve $Er \simeq 1$, v_∞ must be as large as 80 $\mu\mathrm{m\ s^{-1}}$. However, from equation (9) Er is proportional to R_0 and when we take $R_0 = 20$ μm, $v_\infty \simeq 12$ $\mu\mathrm{m\ s^{-1}}$ (smaller than the particle radius per second) is sufficient for $Er \simeq 1$. We also notice that for $\xi_R = 5 \times 10^{-3}$, the hedgehog configuration is stable and in the following calculations we use the equilibrium profile of the hedgehog configuration as the initial condition.

In figure 3, we show how the orientation profile of a nematic liquid crystal around a particle evolves with time after the application of a flow with $|Er| = 0.1$. We find almost no change in the orientation profile, confirming the assumption of fixed director profile in the previous studies dealing with low Ericksen number cases. This result is natural because $|Er| = 0.1$ implies that the viscous force of the fluid is so weak as compared with the elastic force of the liquid crystal that the fluid flow cannot disturb the orientation profile (recall the definition of the Ericksen number given in equation (9)).

We show next in figure 4 the streamline patterns for $|Er| = 0.1$. A small Ericksen number implies in turn that the fluid flow is strongly influenced by the orientational order of the liquid crystal. We notice that in the hydrodynamic equation for the fluid velocity (6), the anisotropy of the viscosity is neglected as in the original version of Olmsted and Goldbart [32]. When the coupling between the orientational order and the fluid flow is absent, that is the term proportional to $1/Er^*$ in equation (6) is dropped, equation (6) with $Re \to 0$ yields the Stokes flow, which is shown in figure 4 as a reference. We find that the deviation of the flow

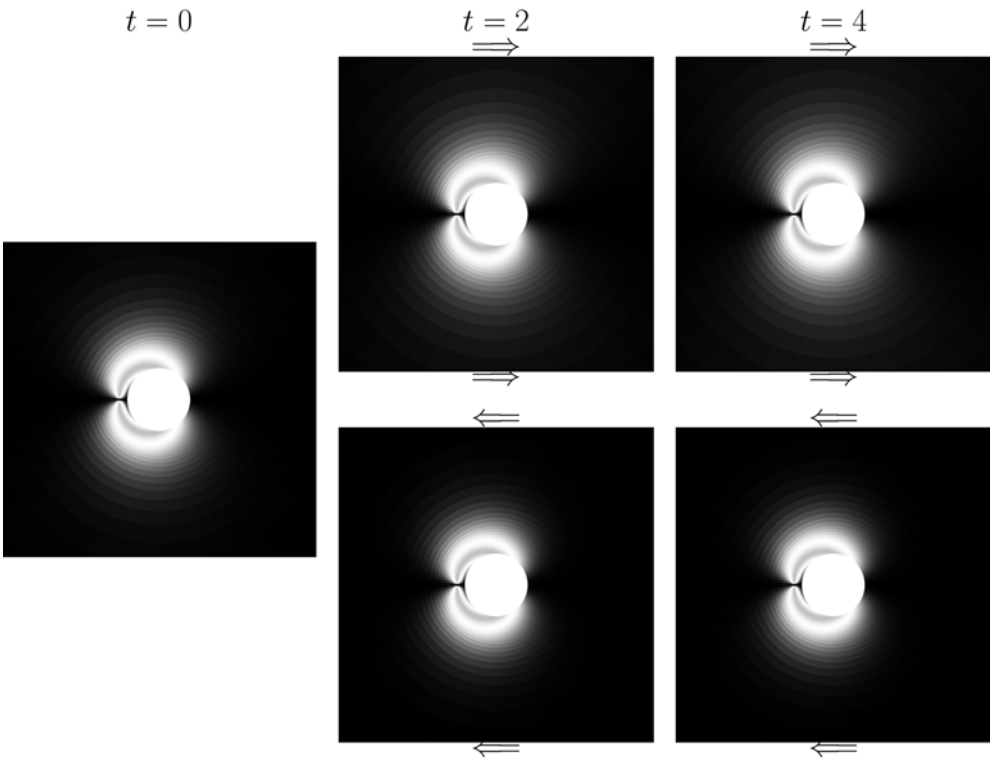

Figure 3. Time evolution of the orientation profile (grey-scale plots of Q_{zz}^2) for $|Er| = 0.1$ with different flow directions. The z-axis, which is parallel to the symmetry axis and the flow direction, is along the horizontal direction. The numbers indicate the time after the application of the flow. The arrows indicate the direction of the flow at infinity relative to the fixed particle.

profile from that of the Stokes flow is significant even in the absence of the anisotropy of the viscosity and that for both directions of the fluid flow, on the right-hand side of the particle, the streamlines get closer to the particle than the Stokes flow. At present our numerical scheme for the determination of the velocity profile heavily relies on the assumption that the viscosity is independent of the position. The incorporation of the anisotropic viscosity should be important to the full understanding of the hydrodynamic behaviour of the liquid crystal and will be the subject of future studies.

We also present the results for an intermediate Ericksen number $|Er| = 1$. In figures 5 and 6 we show the time evolution of the orientation profile and the streamline patterns at $t = 20$, respectively. In contrast to the previous cases with $|Er| = 0.1$, the orientation profiles are strongly distorted by the flow. It is important to notice that while in the case of applying an external field $\tilde{H}$, the free energy is symmetric under the transformation $\tilde{H} \leftrightarrow -\tilde{H}$, the hydrodynamic equations (6) and (7) are not under the transformation $\boldsymbol{v} \rightarrow -\boldsymbol{v}$. Therefore the fluid flows with different directions yield different responses of the orientational order of a liquid crystal as is evident in figure 5. In the first row of figure 5 where the liquid crystal flows from left to right (or from the defect to the particle), the white region with $Q_{zz} = 0$ is enlarged in the right direction. It is intuitively understood that such behaviour of the orientation profile is attributed to convection. When the flow direction is from the particle to the defect, the white region is pushed along the flow direction again by convection. We also find that with the

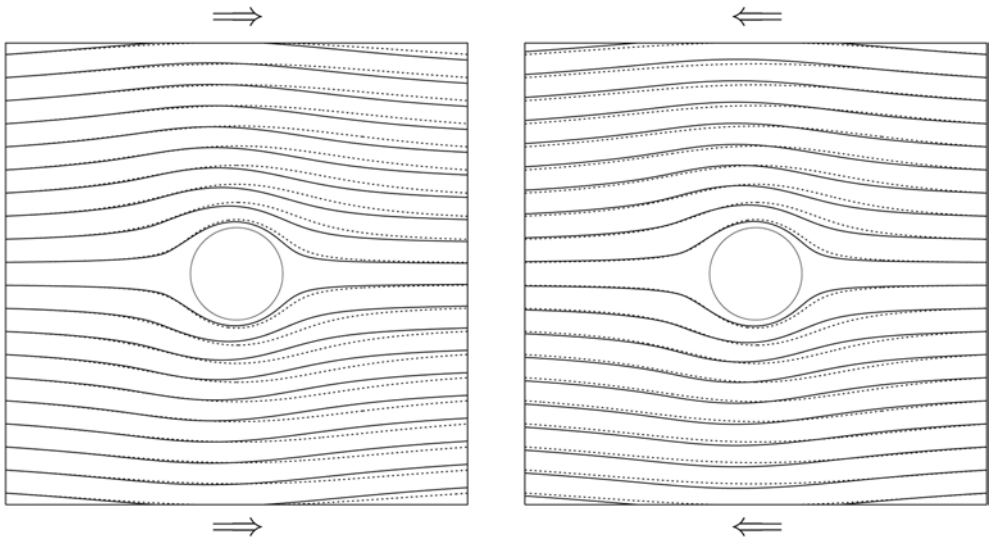

Figure 4. Streamline patterns for $|Er| = 0.1$ with different flow directions at $t = 4$. The arrows indicate the direction of the flow at infinity relative to the fixed particle. The hedgehog is located to the left of the particle as in figure 3. The z-axis, which is parallel to the symmetry axis and the flow direction, is along the horizontal direction. The dotted curves correspond to the Stokes flow.

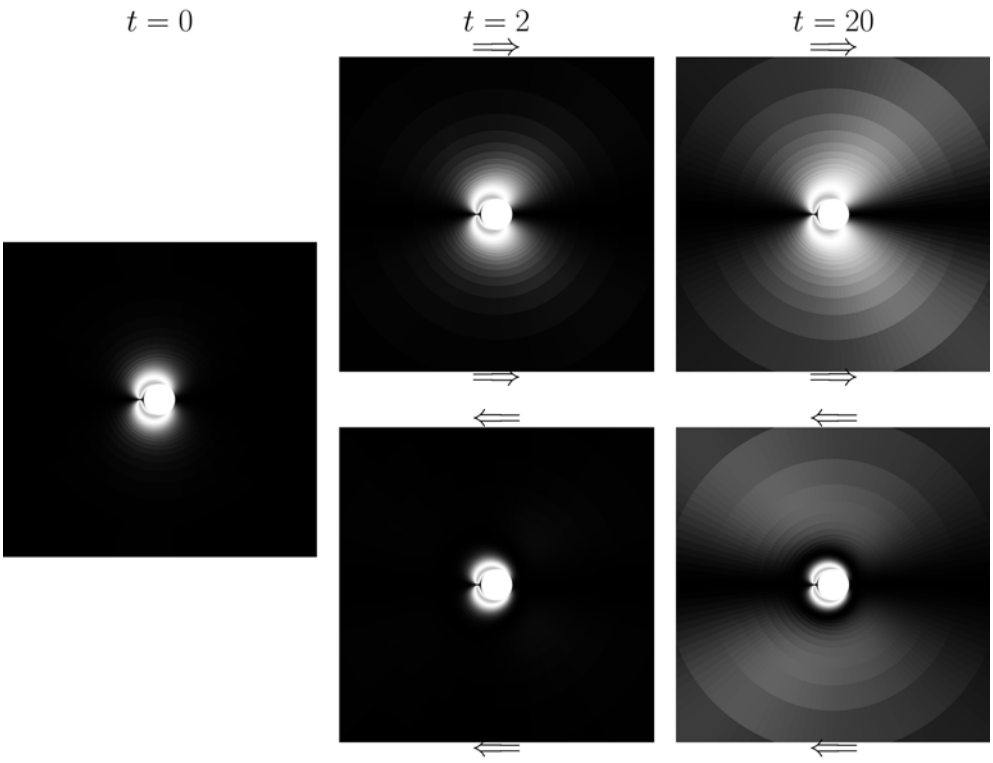

Figure 5. The same as figure 3 for $|Er| = 1$.

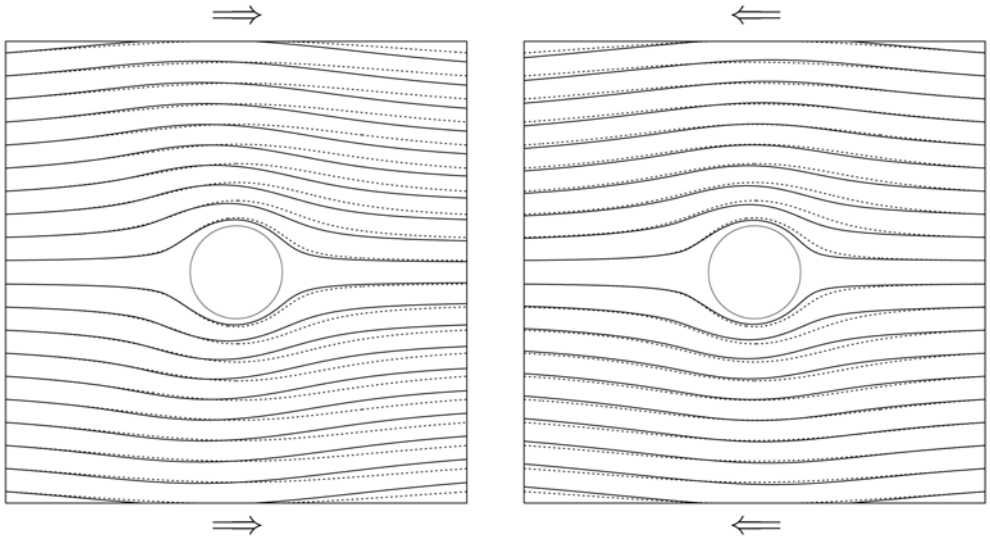

Figure 6. The same as figure 4 for $|Er| = 1$ at $t = 20$.

passage of time, the grey regions appear far from the particle, which indicates that the director deviates from the z direction there. Closer inspection of the numerical results, whose details are not shown here, reveals that such regions appear first to the right of the particle and they become larger by convection. The streamline patterns in figure 6 show deviations from that of the Stokes flow as in the case of $|Er| = 0.1$.

Finally we comment that Stark and Ventzki [30] expect that a hedgehog might be unstable enough to transform to a Saturn ring under a strong flow field with $|Er| \gg 1$. In our preliminary studies with larger Ericksen numbers, however, such a transition has not been observed; in spite of a larger elastic deformation of the liquid crystal the hedgehog defect itself seems stable. At the present stage for the hydrodynamic problem, we use 'fixed' numerical grids with finer grids located around the initial position of the defect core and the mesh rearrangement as in the previous section is not employed here. Therefore significant motion of the defect core cannot be traced in the present scheme (in the calculations presented here, the motion of the defect is so small that it stays within the finest grids allocated initially). Moreover, anisotropic viscosity, which is not incorporated in our study, might be relevant to the stability of a hedgehog defect under flow. Further elaborated studies will be necessary to answer the question whether a hedgehog can be unstable under a flow field.

4. Conclusion

In this paper we presented some of our numerical results as to how external perturbations affect the orientation profile of a nematic liquid crystal around a spherical particle. In particular we focused on the dynamical behaviour of the orientation profile and the topological defects that accompany the particle, which almost no previous numerical work has studied so far.

In the first part of this paper, section 2, we discussed how an external magnetic or electric field influences the orientation profile of a liquid crystal around a particle with a hedgehog defect. We reproduced successfully, with the aid of an adaptive mesh refinement scheme together with the description of the order parameter in a second-rank tensor, the transition

from a hedgehog to a Saturn ring, which was predicted in a previous theory and confirmed in recent experiments. We further made a detailed analysis of the transition processes and found that when the field strength is just above the threshold value for the transition, the hedgehog defect first approaches the particle and after that it opens up to transform itself to a Saturn ring. By contrast, under a stronger field the hedgehog first opens up before approaching the particle. The distance between the defect core and the particle surface becomes smaller gradually until the defect finally takes the Saturn ring configuration. We expect that this difference in the transition process can be checked in carefully controlled experiments.

The second part, section 3, was devoted to the discussion as to how the hedgehog profile of a nematic liquid crystal around a particle is affected by the application of a uniform hydrodynamic flow. For a small Ericksen number, when the viscous force arising from the fluid flow is much smaller than the elastic force of a liquid crystal, almost no effect of the fluid flow on the orientation profile is observed, as expected. The fluid flow in turn is significantly influenced by the coupling with the orientational order and shows a strong deviation from that of the Stokes flow. For an intermediate Ericksen number, the nematic liquid crystal is strongly convected by the fluid flow which results in a significant elastic deformation as compared with the initial profile. In contrast to the cases under a magnetic or electric field, the hydrodynamic equations are not invariant under the transformation $\boldsymbol{v} \leftrightarrow -\boldsymbol{v}$ and therefore the response of the liquid crystal is different under flows with different directions. However, our numerical scheme has not been elaborated enough to give a definite answer to the interesting and important question of whether a uniform hydrodynamic flow can induce a transition of a hedgehog defect, which will be a subject of future studies.

In this paper we dealt with a system that contain one particle and, as noted in the introduction, several authors have been developing numerical schemes that can simulate liquid crystal colloid dispersions with two or more mobile particles. However, we would like to conclude this paper by emphasizing that liquid crystal colloid dispersions still provide a challenge to computational physicists because of the difference in the characteristic lengths associated with particles and liquid crystals together with the coupling between the degrees of freedom of particles and liquid crystals. Much still remains to be investigated, in particular in the dynamical aspects of liquid crystal colloid dispersions.

References

[1] Poulin P, Raghunathan V A, Richetti P and Roux D 1994 *J. Physique* II **4** 1557
[2] Poulin P, Stark H, Lubensky T C and Weitz D A 1997 *Science* **275** 1770
[3] Zapotocky M, Ramos L, Poulin P, Lubensky T C and Weitz D A 1999 *Science* **283** 209
[4] Meeker S P, Poon W C K, Crain J and Terentjev E M 2000 *Phys. Rev.* E **61** R6083
[5] Yamamoto J and Tanaka H 2001 *Nature* **409** 321
[6] Nazarenko V G, Nych A B and Lev B I 2001 *Phys. Rev. Lett.* **87** 075504
[7] Ramaswamy S, Nityananda R, Raghunathan V A and Prost J 1996 *Mol. Cryst. Liq. Cryst.* **288** 175
[8] Ruhwandl R W and Terentjev E M 1997 *Phys. Rev.* E **55** 2958
[9] Lubensky T C, Pettey D, Currier N and Stark H 1998 *Phys. Rev.* E **57** 610
[10] Lev B I and Tomchuk P M 1999 *Phys. Rev.* E **59** 591
[11] Poulin P and Weitz D A 1998 *Phys. Rev.* E **57** 626
[12] Mondain-Monval O, Dedieu J C, Gulik-Krzywicki T and Poulin P 1999 *Eur. Phys. J.* B **12** 167
[13] Gu Y and Abbott N L 2000 *Phys. Rev. Lett.* **85** 4719
[14] Ruhwandl R W and Terentjev E M 1997 *Phys. Rev.* E **56** 5561
[15] Stark H 1999 *Eur. Phys. J.* B **10** 311
Stark H 2001 *Phys. Rep.* **351** 387
[16] Billeter J L and Pelcovits R A 2000 *Phys. Rev.* E **62** 711
[17] Andrienko D, Germano G and Allen M P 2001 *Phys. Rev.* E **63** 041701
[18] Fukuda J and Yokoyama H 2001 *Eur. Phys. J.* E **4** 389

[19] Fukuda J, Yoneya M and Yokoyama H 2002 *Phys. Rev.* E **65** 041709
[20] Fukuda J, Yoneya M and Yokoyama H 2003 *Mol. Cryst. Liq. Cryst.* at press
[21] Yamamoto R 2001 *Phys. Rev. Lett.* **87** 075502
Yamamoto R 2004 *J. Phys.: Condens. Matter* **16** S1945
[22] Good K, Care C M, Halliday I and Cleaver D J 2002 *19th Int. Liquid Crystal Conf. (Edinburgh, UK)*
[23] Loudet J C and Poulin P 2001 *Phys. Rev. Lett.* **87** 165503
[24] Loudet J C, Mondain-Monval O and Poulin P 2002 *Eur. Phys. J.* E **7** 205
[25] de Gennes P G and Prost J 1993 *The Physics of Liquid Crystals* 2nd edn (Oxford: Oxford University Press)
[26] Heuer H, Kneppe H and Schneider F 1992 *Mol. Cryst. Liq. Cryst.* **214** 43
[27] Ruhwandl R W and Terentjev E M 1996 *Phys. Rev.* E **54** 5204
[28] Chono S and Tsuji T 1998 *Mol. Cryst. Liq. Cryst.* **309** 217
[29] Stark H and Ventzki D 2001 *Phys. Rev.* E **64** 031711
[30] Stark H and Ventzki D 2002 *Europhys. Lett.* **57** 60
Stark H, Ventzki D and Reichert M 2003 *J. Phys.: Condens. Matter* **15** S191
[31] Hess S 1975 *Z. Naturf.* a **30** 728
[32] Olmsted P D and Goldbart P 1990 *Phys. Rev.* A **41** 4578
Olmsted P D and Goldbart P 1992 *Phys. Rev.* A **46** 4966
[33] Qian T and Sheng P 1998 *Phys. Rev.* E **58** 7475
[34] Pleiner H, Liu M and Brand H R 2002 *Rheol. Acta* **41** 375
[35] Stark H and Lubensky T C 2003 *Phys. Rev.* E **67** 061709